Published in final edited form as:
Atmos Chem Phys. 2020 November 20; 20(22): 14077–14090. doi:10.5194/acp-20-14077-2020.

Chemical composition, structures, and light absorption of N-containing aromatic compounds emitted from burning wood and charcoal in household cookstoves

Mingjie Xie[1], **Zhenzhen Zhao**[1], **Amara L. Holder**[2], **Michael D. Hays**[2], **Xi Chen**[2], **Guofeng Shen**[3], **James J. Jetter**[2], **Wyatt M. Champion**[4], **Qin'geng Wang**[5]

[1]Collaborative Innovation Center of Atmospheric Environment and Equipment Technology, Jiangsu Key Laboratory of Atmospheric Environment Monitoring and Pollution Control, School of Environmental Science and Engineering, Nanjing University of Information Science & Technology, 219 Ningliu Road, Nanjing 210044, China

[2]Office of Research and Development, U.S. Environmental Protection Agency, 109 T.W. Alexander Drive, Research Triangle Park, NC 27711, USA

[3]Laboratory for Earth Surface Processes, College of Urban and Environmental Sciences, Peking University, Beijing 100871, China

[4]Oak Ridge Institute for Science and Education (ORISE) Postdoctoral Fellow at U.S. Environmental Protection Agency, Office of Research and Development, Air Methods and Characterization Division, 109 T.W. Alexander Drive, Research Triangle Park, NC 27711, USA

[5]State Key Laboratory of Pollution Control and Resource Reuse, Nanjing University, Nanjing 210023, China

Abstract

N-containing aromatic compounds (NACs) are an important group of light-absorbing molecules in the atmosphere. They are often observed in combustion emissions, but their chemical formulas and structural characteristics remain uncertain. In this study, red oak wood and charcoal fuels were burned in cookstoves using the standard water boiling test (WBT) procedure. Submicron aerosol particles in the cookstove emissions were collected using quartz (Q_f) and polytetrafluoroethylene (PTFE) filter membranes positioned in parallel. A back-up quartz filter (Q_b) was also installed downstream of the PTFE filter to evaluate the effect of sampling artifact on NACs measurements. Liquid chromatography-mass spectroscopy (LC-MS) techniques identified seventeen NAC chemical formulas in the cookstove emissions. The average concentrations of total NACs in Q_b

Correspondence to: Mingjie Xie, mingjie.xie@colorado.edu; mingjie.xie@nuist.edu.cn, Tel: +1-18851903788; Fax: +86-25-58731051; Mailing address: 219 Ningliu Road, Nanjing, Jiangsu, 210044, China.

Author contribution

MX and AH designed the research. MX, ZZ, and XC performed the experiments. GS, WC, and JJ managed cookstove emission tests and sample collection. MX and MH analyzed the data and wrote the paper with significant contributions from AH and QW.

Competing interests

The authors declare that they have no conflict of interest.

Disclaimer

The views expressed in this article are those of the authors and do not necessarily represent the views or policies of the U.S. Environmental Protection Agency.

samples (0.37 ± 0.31 – 1.79 ± 0.77 μg m^{-3}) were greater than 50% of those observed in the Q_f samples (0.51 ± 0.43 – 3.91 ± 2.06 μg m^{-3}), and the Q_b to Q_f mass ratios of individual NACs had a range of 0.02 – 2.71, indicating that the identified NACs might have substantial fractions remaining in the gas-phase. In comparison to other sources, cookstove emissions from red oak or charcoal fuels did not exhibit unique NAC structural features, but had distinct NACs composition. However, before identifying NACs sources by combining their structural and compositional information, the gas-particle partitioning behaviors of NACs should be further investigated. The average contributions of total NACs to the light absorption of organic matter at λ = 365 nm (1.10 – 2.57%) in Q_f and Q_b samples (10.7 – 21.0%) are up to 10 times larger than their mass contributions (Q_f 0.31 – 1.01%, Q_b 1.08 – 3.31%), so the identified NACs are mostly strong light absorbers. To explain more sample extracts absorption, future research is needed to understand the chemical and optical properties of high molecular weight (e.g., MW > 500 Da) entities in particulate matter.

1 Introduction

In the developing world, 2.8 billion people burn solid fuels in household cookstoves for domestic activities such as heating and cooking (Bonjour et al., 2013). A variety of gaseous and particle-phase pollutants — carbon monoxide (CO), nitrogen oxides (NO_X), volatile organic compounds (VOCs), fine particulate matter with aerodynamic diameter ≤ 2.5 μm ($PM_{2.5}$), black carbon (BC), organic carbon (OC), etc. — are emitted from cookstoves largely due to incomplete combustion (Jetter et al., 2012; Shen et al., 2012; Wathore et al., 2017). In China, the relative contributions of residential coal and biomass burning (BB) to annual $PM_{2.5}$ emissions decreased from 47% (4.32 Tg) in 1990 to 34% (4.39 Tg) in 2005 due to the growth in industrial emissions (Lei et al., 2011). Although, more than half of BC (> 50 %) and OC (> 60 %) emissions are attributed to residential coal and BB in both China and India (Cao et al., 2006; Klimont et al., 2009; Lei et al., 2011).

Household solid fuel combustion is a leading human health risk, especially for women and children who tend to spend more time indoors than men (Anenberg et al., 2013). Estimates show that exposures to $PM_{2.5}$ from domestic solid fuel combustion caused 3.9 million premature deaths and ~4.8% of lost healthy life years (Smith et al., 2014). In addition, the emissions of carbonaceous aerosols from cookstoves can affect the Earth's radiative balance by absorbing and scattering incoming solar radiation (Lacey and Henze, 2015; Aunan et al., 2009). BC is the most efficient light absorber in the atmosphere, while the total aerosol absorption, including that from OC, is still highly uncertain (Yang et al.,2009; Park et al., 2010; Feng et al., 2013; Wang et al., 2014; Tuccella et al., 2020). Multiple field and laboratory studies have demonstrated that OC in both primary PM emissions (e.g., biomass and fossil fuel combustions) and secondary organic aerosol (SOA) feature a range of absorptivity in the near ultraviolet (UV) and short visible wavelength regions (Nakayama et al., 2010; Forrister et al., 2015; Lin et al., 2015; De Haan et al., 2017; Xie et al., 2017a, b, 2018). The light absorbing OC fraction is often referred to as "brown carbon" (BrC). Unlike open BB (e.g., forest, grassland, and cropland fires) — one of the most important primary sources for organic aerosols (Bond et al., 2004) — the light absorption of BrC from household cookstove emissions is rarely investigated. Sun et al. (2017) found that the BrC

absorption from residential coal burning accounted for 26.5% of the total aerosol absorption at 350~850 nm. BrC from wood combustion in cookstoves has a greater mass specific absorption than that from open BB over the wavelength range of 300 – 550 nm (Xie et al., 2018). These results suggest that cookstove emissions may also be an important BrC source, which needs to be accounted for separately from open BB.

Organic molecular markers (OMMs) are commonly used in receptor-based source apportionment of carbonaceous aerosols (Jaeckels et al., 2007; Shrivastava et al., 2007; Xie et al., 2012). Polycyclic aromatic hydrocarbons (PAHs) and their derivatives are a group of OMMs with light absorption properties dependent on ring number or the degree of conjugation (Samburova et al., 2016). As discussed in Xie et al. (2019), PAHs are generated from a multitude of combustion processes (e.g., BB, fossil fuel combustion) (Chen et al., 2005; Riddle et al., 2007; Samburova et al., 2016), and their ubiquitous nature makes them less than ideal OMMs for BrC source attribution. Because of the specific toxicological concern raised by PAHs — they are mutagenic and carcinogenic [International Agency for Research on Cancer (IARC), 2010] — source emission factors (EFs), ambient levels, and potential health effects of PAHs are investigated exhaustively (Ravindra et al., 2008; Kim et al., 2013). Similar to PAHs, N-containing aromatic compounds (NACs) are a group of BrC chromophores commonly detected in ambient PM and source emissions. Zhang et al. (2013) and Teich et al. (2017) calculated the absorption of individual NACs in aqueous extracts of ambient PM, the total of which explained ~3% of the bulk extract absorption at 365 – 370 nm. With the same approach, Xie et al. (2017a, 2019) found that the absorbance due to NACs in BB or secondary OC was 3 – 10 times higher than their mass contributions. Lin et al. (2016, 2017) estimated an absorbance contribution of 50 – 80% from NACs in BB OC directly from their high-performance liquid chromatography (HPLC)/photodiode array (PDA) signals, which are subject to considerable uncertainty due to the co-elution of other BrC chromophores (e.g., PAHs and their derivatives). These results indicate that NACs are strong BrC chromophores, but the estimation of their contributions to BrC absorption depends largely on how well they are chemically characterized. Nitrophenols, methyl nitrophenols, nitrocatechols and methyl nitrocatechols (including isomers) are typical atmospheric NACs (Claeys et al., 2012; Desyaterik et al., 2013; Zhang et al., 2013). These NACs can be generated from BB (Lin et al., 2016, 2017; Xie et al., 2019), fossil fuel combustion (Lu et al., 2019), and the reactions of aromatic volatile organic compounds (VOCs) with reactive nitrogen species (e.g., NO_X) (Xie et al., 2017a), and are not unique to specific sources (e.g., BB). By using a HPLC interfaced to a diode array detector (DAD) and quadrupole (Q) time-of-flight mass spectrometer (ToF-MS), Xie et al. (2019) found that BB NACs contain methoxy and cyanate groups. Nitronaphthol, nitrobenzenetriol, and methyl nitrobenzenetriol are characteristic NACs for NO_X-based chamber reactions of naphthalene, benzene, and *m*-cresol, respectively (Xie et al., 2017a). Yet, few studies have investigated the composition of NACs from household cookstove emissions (Fleming et al., 2018; Lu et al., 2019).

The present study aims to characterize NACs in $PM_{2.5}$ from burning red oak and charcoal in a variety of cookstoves and calculate their contributions to bulk OC absorption. The absorption of OC in solvent extracts of cookstove emissions were measured in our previous work (Xie et al., 2018). Presently, NACs are identified and quantified using an earlier

described HPLC/DAD-Q-ToF-MS system. In addition, the NACs adsorbed on a backup quartz filter downstream of a polytetrafluoroethylene (PTFE) membrane filter are analyzed, to evaluate the potential for sampling artifacts of $PM_{2.5}$ NACs on the bare quartz filter in parallel. This work unveils BrC composition at a molecular level and increases the understanding of BrC chromophores and their sources. It also shows that further identification of large molecules (e.g., > 500 Da) may better explain BrC absorption in the particle phase.

2 Methods

2.1. Cookstove emissions sampling

The cookstove emission test facility, fuel-cookstove combinations, water boiling test (WBT) protocol, and $PM_{2.5}$ emissions sampling were described previously in Jetter and Kariher (2009) and Jetter et al. (2012). Briefly, the cookstove emission tests were performed at the United States Environmental Protection Agency (US EPA) cookstove test facility in Research Triangle Park, NC, USA. Red oak wood and lump charcoal were burned in fuel-specific cookstoves under controlled conditions. Emissions tests for each fuel-cookstove combination were performed in triplicate. The WBT protocol (version 4) (Global Alliance for Clean Cookstoves, 2014) is designed to measure cookstove power, energy efficiency, and fuel use, and contains cold-start (CS) high power, hot-start (HS) high power, and simmer (SIM) low power phases. Both CS and HS phases are defined by the duration between the ignition and the water boils. The CS phase starts with the cookstove, pot, and water at ambient temperature; the HS immediately follows the CS with the cookstove hot but the pot and water at ambient temperature; and the SIM phase is defined by a 30-min time period with the cookstove hot and water temperature maintained at 3 °C below the boiling point. Low moisture (~10%) oak and charcoal fuels were burned with five specific-designed cookstove types (Tables S1 and S2); high moisture (~30%) oak fuels were burned in one cookstove (Jiko Poa, BURN Manufacturing, Kenya). A brief description of each fuel-specific cookstove was given in supplementary information (Text S1). Gaseous pollutant (e.g., CO, methane (CH_4)) emissions were monitored continuously, and $PM_{2.5}$ filter samples were collected during each test phase of the WBT protocol. The modified combustion efficiency (MCE), defined as $CO_2/(CO_2 + CO)$ on a molar basis, was calculated and discussed in Xie et al. (2018). A quartz-fiber filter (Q_f) and a PTFE membrane filter positioned in parallel collected $PM_{2.5}$ isokinetically at a flow rate of 16.7 L min^{-1}. The adsorption artifact of Q_f was evaluated using a quartz-fiber back-up filter (Q_b) installed downstream of the PTFE filter during $PM_{2.5}$ sampling.

2.2. Chemical analysis

The OC and elemental carbon (EC) emissions and UV-Vis light absorption properties (BrC) of methanol-extracted cookstove particles were reported in Xie et al. (2018). Details for determinations of OCEC concentrations and BrC absorption were provided in supplementary information (Text S2). Except the 3-stone fire, EFs of OC and EC at the SIM phase were substantially lower than those at high power phases (CS and HS), so the BrC absorption from red oak and charcoal burning were primarily measured for CS- and HS-phase samples in Xie et al. (2018). The SIM-phase samples were analyzed only for red oak

burning in a 3-stone fire. This test had comparable OC emissions between CS- and SIM-phase combustions, and CS and HS phases of the 3-stone fire were typically similar and could not be separated (Xie et al., 2018). In the current work, the same emission samples were selected for the analysis of NACs, and the three SIM-phase samples from the 3-stone fire were treated as HS-phase samples of other cookstove tests. Tables S1 and S2 summarized the measurement results of Q_f and Q_b, respectively, for each fuel-cookstove combination, including concentrations of carbon contents and light-absorbing properties of sample extracts. As the light absorption of BB BrC is expected to depend largely on burn conditions (Saleh et al., 2014; Pokhrel et al., 2016), the MCE and EC/OC ratio, two indicators of burn conditions, are also given in Table S1.

The Q_f and Q_b, sample extraction and subsequent analysis for NACs were conducted as described in Xie et al. (2019). In brief, an aliquot of each filter sample was pre-spiked with 250 ng nitrophenol-d4 (internal standard) and extracted ultrasonically twice for 15 min in 3-5 mL of methanol. After filtration (30 mm diameter ×0.2 μm pore size, PTFE filter, National Scientific Co. Ltd, TN, USA), the extract volume was reduced to ~500 μL with rotary evaporation prior to HPLC/DAD-MS (Q-ToF) analysis. The NACs targeted in this work were chromatographed using an Agilent 1200 Series HPLC equipped with a Zorbax Eclipse Plus C18 column (2.1 mm × 100 mm, 1.8 μm particle size; Agilent Technologies, CA, USA). The gradient separation was performed using water (eluent A) and methanol (eluent B) containing 0.2% acetic acid (v/v) with a total flow rate of 0.2 mL min^{-1}. The eluent B fraction was held at 25% for 3 min, increased to 100% over the next 7 min, where it was held for 22 min, and then returned to 25% over 5 min. An Agilent 6520 Q-ToF MS equipped with a multimode ion source operating in electrospray ionization (ESI) negative (−) mode was used to determine the chemical formula, molecular weight (MW), and quantity of each target compound. All sample extracts were analyzed in full scan mode over 40–1000 Da. A mass accuracy of ± 10 ppm was selected for compound identification and quantification. Samples with individual NACs exhibiting the highest MS signal intensities in full scan mode were re-examined in targeted MS-MS mode using a collision-induced dissociation (CID) technique. The MS-MS spectra of target NACs $[M\text{-}H]^-$ ions were acquired to deduce structural information. Similar to bulk carbon and light absorption measurements, NACs were primarily determined for CS- and HS-phase samples with substantial OC loadings.

Due to the limited availability of authentic standards, many of the NACs identified in cookstove combustion samples were quantified using surrogate compounds with similar MW or structures. An internal standard method with a 9-point calibration curve (~0.01 – 2 ng μL^{-1}) was applied for quantification of concentrations. The compounds represented by each identified NAC formula were quantified individually and combined to calculate the mass ratio of total NACs to OC (μg m^{-3}) × 100% ($tNAC_{OC}$%). Presently, the organic matter (OM) to OC ratio was not measured or estimated for cookstove combustion emissions, so $tNAC_{OC}$% could be up to 2 times greater than the contributions of NACs to OM (Reff et al., 2009; Turpin and Lim, 2001). Table S3 lists the chemical formulas, proposed structures, and standard assignments for the NACs identified here. The quality assurance and control (QA/QC) procedures for filter extraction and instrumental analysis were the same as Xie et al. (2017a, 2019). NACs were not detected in field blank and background samples. The

average recoveries of NAC standards on pre-spiked blank filters ranged from 75.1% to 116%, and the method detection limit had a range of 0.70–17.6 pg.

2.3. Data analysis

In Xie et al. (2017a), the DAD measurement directly identified the chemical compounds in chamber SOA responsible for light absorption in the near UV and visible light ranges. However, no light absorption from individual NACs was detected in the DAD chromatograms from open BB (Xie et al., 2019) and cookstove emissions (this work). So the contributions of individual NACs to light absorption coefficient (Abs_{λ}, Mm^{-1}) for each sample extract at 365 nm ($Abs_{365,iNAC}$%) were calculated using the method described in Xie et al. (2017a, 2019):

$$\mathrm{Abs}_{365,\,\mathrm{iNAC}}\,\% = \frac{\mathrm{C}_{\mathrm{iNAC}} \times \mathrm{MAC}_{365,\,\mathrm{iNAC}}}{\mathrm{Abs}_{365}} \times 100\,\% \quad (1)$$

where C_{iNAC} is the mass concentration (ng m^{-3}) of individual NACs, and $MAC_{365,iNAC}$ is the mass absorption coefficient (MAC_{λ}, $m^2\ g^{-1}$) of individual NACs at 365 nm. Abs_{365} is the light absorption coefficient (Mm^{-1}) of each sample extract at 365 nm, and has been widely used to represent BrC absorption (Chen and Bond, 2010; Hecobian et al., 2010; Liu et al., 2013). Each NAC compound was assumed to absorb as a standard (Table S3), of which the $MAC_{365,iNAC}$ value was obtained from Xie et al. (2017a, 2019) and listed in Table S4. In this work, Student's *t*-test was used to determine if the means of two sets of data are significantly different from each other, and a p value less than 0.05 indicates significant difference.

3 Results and discussion

3.1 Summary of total NACs concentration from cookstove emissions

Table 1 summarizes the average concentrations of total NACs and average $tNAC_{OC}$% for Q_f and Q_b by fuel type and WBT phase. The EFs of total NACs shown in Table S5 were obtained by multiplying the EFs of OC and $tNAC_{OC}$%. Filter samples of emissions from burning red oak wood had significantly ($p < 0.05$) higher average total NAC concentrations and $tNAC_{OC}$% than the charcoal burning samples. Wood burning generates more volatile aromatic compounds (e.g., phenols, PAHs) than charcoal burning (Kim Oanh, et al., 1999), and NACs can form when aromatic compounds and reactive nitrogen (e.g., NO_X) are present during solid fuel combustion (Lin et al., 2016, 2017). While burning red oak, emissions from the CS and HS phases show similar average NAC concentrations, $tNAC_{OC}$%, and NAC EFs (Tables 1 and S5). Additionally, burning low moisture red oak in the Jiko Poa stove had higher $tNAC_{OC}$% than burning high moisture red oak (Tables S6 and S7), but the difference was not significant ($p > 0.05$). Thus, the NAC emissions from red oak burning are less likely influenced by WBT phase, and the effect of fuel moisture content needs further investigation. For charcoal fuel samples, compared with the CS-phase, the HS-phase shows significantly higher ($p < 0.05$) average NAC concentrations and EFs. This is likely due to the increase in OC with the HS phase (Tables 1 and S5), as the average $tNAC_{OC}$% values are much closer for the CS- (0.40 ± 0.25%) and HS-phases (0.31 ± 0.21%).

Several studies have placed a quartz-fiber filter behind a PTFE filter to evaluate the positive adsorption artifact — adsorption of gas-phase compounds onto particle filter media, "blow-on" effect (Peters et al., 2000; Subramanian et al., 2004; Watson et al., 2009; Xie et al., 2014). This method is expected to provide a consistent estimate irrespective of sampling time, but may over correct the positive artifact by 16–20% due to volatilization of OC off the upstream PTFE filter (negative artifact, "blow-off" effect) (Subramannian et al., 2004). A denuder upstream of the filter for gas sampling was used to avoid positive artifact in several studies (Ding et al., 2002; Ahrens et al., 2012). This approach can generate large negative artifacts by altering the gas-particle equilibrium after the denuder, and a denuder efficiency of 100% might not be guaranteed (Kirchstetter et al., 2001; Subramanian et al., 2004). The present study is the first to consider sampling artifact when measuring semivolatile NACs. This concept merits consideration as quantification of particle-phase NACs may be subject to large uncertainty. Table 1 shows that the average concentrations of total NACs on Q_b (0.37 ±0.31 – 1.79 ± 0.77 μg m^{-3}) are greater than 50% and 80% of those on Q_f (0.51 ± 0.43 – 3.91 ± 2.06 μg m^{-3}) for red oak and charcoal burning, respectively. The average Q_b to Q_f ratio in percentage using OC concentrations is 2-3 times lower (14.8 ± 3.87 – 38.8 ± 18.9%). Hence, the NACs identified in this work are present in the relatively volatile bulk OC fraction emitted from cookstoves, and the NACs in the Q_f samples may also be present in the gas-phase in the atmosphere. Charcoal burning emissions show even higher (p <0.05) Q_b to Q_f total NAC mass ratios (CS 84.1 ± 38.0%, HS 140 ± 52.9%) than red oak burning (CS 50.8 ± 13.4%, HS 53.4 ± 26.2%), which is largely due to the higher OC loads on Q_f from red oak burning. Xie et al. (2018) assumed previously that the Q_b-adsorbed OC represented the positive sampling artifact only, and adjusted the light absorbing properties of OC on Q_f by subtracting Abs_{365} and OC of Q_b samples directly. In this study, the high Q_b to Q_f ratios of total NACs indicate that the volatilization of NACs from upstream PTFE filter cannot be neglected, but the relative contributions of positive and negative artifacts to Q_b measurements are unknown. Therefore, the measurement results of NACs in Q_f and Q_b samples were provided separately, and no correction was conducted for Q_f measurements in this work. Since the gaseous NACs adsorbed in Q_b samples depends on Q_f loadings, $tNAC_{OC}$% and total NACs concentrations in each Q_f-Q_b pair from matching tests are significantly correlated (p < 0.05, Fig. S1a, b, d, and e).

Along with modified combustion efficiency (MCE), the EC/OC and BC/OA (organic aerosol) ratios were used previously as indicators of biomass burning conditions (McMeeking et al., 2014; Pokhrel et al., 2016). Here the burn condition indicates general flame intensity or combustion temperature (Chen and Bond, 2010; Saleh et al., 2014), and is parameterized to investigate combustion processes (e.g., pyrolysis). The MCE, EC/OC and BC/OA ratios are key to understanding particulate OC absorptivity (Saleh et al., 2014; Lu et al., 2015) and NACs formation from open BB (Xie et al., 2019). Presently, the relationships of $tNAC_{OC}$% versus EC/OC for Q_f samples are shown in Fig. S1c and f by fuel type. Because no significant difference was observed for average total NACs concentrations, $tNAC_{OC}$%, and EC/OC ratios when testing CS- versus HS- phases during red oak fuel burning, the CS- and HS-phases were pooled for a regression analysis. The $tNAC_{OC}$% of Q_f samples positively correlate (r = 0.83, p < 0.05) with EC/OC for red oak burning (Fig. S1c), as observed in Xie et al. (2019) for open BB, which suggests that burn conditions influence

NACs formation during BB. Note that the NAC concentrations on Q_f were possibly adsorbed while in a gaseous state, while EC is particle phase.

In Table S1, the MCE values of charcoal burning indicate that the HS-phase is more smoldering than the CS-phase. However, the average $tNAC_{OC}$% values showed no significant difference ($p = 0.29$) between HS and CS phases. Like MAC_{365} and $Å_{abs}$ in Q_f samples for charcoal burning (Xie et al., 2018), $tNAC_{OC}$% derived from the same samples did not correlate with EC/OC ratios in this work (Fig. S1f). Xie et al. (2018) found that the HS-phase for charcoal burning had average OC EFs 5–10 times higher than the CS-phase, while the EC EFs decreased by more than 90% from the CS- to HS-phase. Furthermore, no correlation has been observed between MCE and EC/OC for charcoal burning at the HS-phase. So, the EC/OC for charcoal burning tends to depend more on the initial temperature in the cookstove than MCE variations, and cannot be used to predict burn conditions, BrC absorption, or NACs formation.

3.2 Composition of NACs in Q_f and Q_b

During solid fuel combustion, NACs may form from aromatic compounds (e.g., substituted phenols) and reactive nitrogen species (e.g., NH_3, NO_X, and HONO) in both the gas- and particle-phase (Harrison et al., 2005; Kwamena and Abbatt, 2008; Lu et al., 2011; Lin et al., 2016, 2017). Aromatic hydrocarbons are produced during fuel pyrolysis (Simoneit et al., 1993; Simoneit, 2002; Kaal et al., 2009). Oxidation of fuel derived nitrogen, rather than molecular nitrogen in air, is the major formation pathway of reactive nitrogen species (Glarborg et al., 2003).

Presently, seventeen chemical formulas were identified as NACs in cookstove emissions, several of which are widely observed in ambient air and open BB particles (e.g., $C_6H_5NO_3$, $C_6H_5NO_4$) (Claeys et al., 2012; Zhang et al., 2013; Lin et al., 2016, 2017; Xie et al., 2019). Figure 1 shows the average concentrations (ng m^{-3}) of individual NACs in Q_f and Q_b samples by fuel type and WBT phase. The corresponding average mass ratios of individual NACs to OC × 100% ($iNAC_{OC}$%) are exhibited in Fig. S2. Details of the NACs composition expressed in $iNAC_{OC}$% for each fuel-cookstove experiment are given in Tables S6-S9.

Generally, the CS and HS phases have consistent NAC profiles for red oak combustion (Figs. 1a, b and S2a, b). $C_{10}H_7NO_3$ (CS-Q_f 1003 ± 803 ng m^{-3}, HS-Q_f 1149 ± 1053 ng m^{-3}) and $C_8H_5NO_2$ (CS-Q_f 712 ± 921 ng m^{-3}, HS-Q_f 1185 ± 1761 ng m^{-3}) have the highest average concentrations on Q_f, followed by $C_{11}H_9NO_3$, $C_{10}H_{11}NO_5$, and $C_{11}H_{13}NO_5$. However, $C_8H_5NO_2$ was only detected in emission samples of Jiko Poa among the five wood stoves (Tables S6 and S7). Not considering $C_8H_5NO_2$, Q_b samples of red oak combustion emissions have similar NACs profiles and characteristic species (e.g., $C_{10}H_7NO_3$, $C_{11}H_9NO_3$) as Q_f samples, and the individual NAC distributions in Q_b to Q_f samples are similar between the CS- and HS-phases (Fig. 1a, b). It appears that the formation of NACs from red oak burning in cookstoves depends largely on burn conditions reflected by EC/OC ratios (Fig. S1c) rather than WBT phases. Among the 17 identified NACs from red oak burning, $C_8H_5NO_2$ and $C_{11}H_{13}NO_6$ have the lowest Q_b to Q_f ratios (2.03 – 9.80%, Fig. 1a, b), indicating their low volatility. The low volatility of $C_{11}H_{13}NO_6$ might be due to its relatively high MW; while $C_8H_5NO_2$ has the second lowest MW and its structure likely

contains functional groups that decrease vapor pressure (e.g., carboxyl group) (Donahue et al., 2011).

Charcoal burning generated high abundances of $C_8H_9NO_5$, $C_{11}H_9NO_3$, and $C_{10}H_7NO_3$ for both CS (86.6 ± 98.7 – 170 ± 200 ng m^{-3}) and HS (97.1 ± 38.5 – 178 ± 104 ng m^{-3}) phases (Figs. 1c, d and S2c, d). Only one of the five charcoal stoves (Éclair, GIZ, Bonn, Germany) emitted $C_8H_5NO_2$, which was not detected on Q_b for charcoal combustions (Tables S8 and S9). Average concentrations of $C_8H_9NO_5$, $C_{11}H_9NO_3$, and $C_{10}H_7NO_3$ in the Q_b (62.0 ± 64.9 – 198 ± 115 ng m^{-3}) and Q_f samples were comparable. However, the $iNAC_{OC}$% of these compounds are 1.45 ± 0.68 – 5.16 ± 2.84 times higher in Q_b ($iNAC_{OC}$%, 0.11 ± 0.18 – 0.46 ± 0.69%) than in Q_f samples (0.052 ± 0.067 – 0.14 ± 0.15%). High levels of $C_6H_5NO_4$, $C_7H_7NO_4$, and $C_8H_9NO_4$ were also observed in the HS phase for charcoal burning (Fig. 1d). These compounds in Q_b samples had average concentrations (222 ± 132 – 297 ± 277 ng m^{-3}) 22.6 – 80.8% higher than in Q_f samples (150 ± 118 – 181 ± 111 ng m^{-3}). As such, the charcoal HS phase generates more low MW NACs (e.g., $C_6H_5NO_4$, $C_7H_7NO_4$) than the CS phase, and the initial temperature in the cookstove has an impact on NAC formation from charcoal burning.

As mentioned in section 3.1, using a Q_b has been widely applied to evaluate the positive sampling artifact for OC and semivolatile organic compounds. This method might only work for bulk PM, OC, and low volatile organic compounds, of which the concentrations in Q_b samples are much lower than Q_f samples and usually presumed to be due to positive adsorption artifacts only (Subramanian et al., 2004; Watson et al., 2009). In this work, the average Q_b to Q_f mass ratios of the 17 individual NACs ranged from 50.8 ± 13.4% to 140 ± 52.9%, comparable to *n*-alkanes with carbon number ≤ 21 (e.g., henicosane; 26.3 – 163%) and PAHs with benzene ring number ≤ 4 (e.g., fluoranthene; 46.3 – 134%) in the ambient of urban Denver (Xie et al., 2014). Xie et al. (2014) found that the gas-phase concentrations of *n*-alkanes and PAHs with vapor pressure greater than henicosane and fluoranthene were comparable or higher than their particle-phase concentrations. The vapor pressure of five NACs standards at 25 °C ($p^{\circ,*}_{L}$) were predicted using the US EPA Toxicity Estimation Software Tool (T.E.S.T) and listed in Table S10. Their $p^{\circ,*}_{L}$ values are mostly higher than henicosane and fluoranthene (~10^{-8} atm; Xie et al., 2013, 2014). Then the identified NACs in this study may have substantial fractions remaining in the gas phase. As the evaporation of NACs from the upstream filter (negative artifact) is unknown, the particle-phase NAC concentrations cannot be calculated by simply subtracting Q_b measurements from those of Q_f. Considering that most of the Q_f and Q_b samples were collected near ambient temperature (Table S2, ~25 °C), the composition of NACs derived from Q_f measurements alone can be biased due to the lack of gas-phase measurements. Future work is needed to evaluate the composition of NACs from emission sources in both the particle and gas phases.

3.3 Identification of NACs structures

Figures S3 and S4 exhibited extracted ion chromatograms (EICs) and MS-MS spectra of the 17 identified NACs. For comparison, the MS-MS spectra of standard compounds used in this work are obtained from Xie et al. (2017a, 2019) and shown in Fig. S5. Among all identified

NAC formulas, $C_{10}H_7NO_3$ was detected in each fuel-cookstove experiment (Tables S6 - S9) and showed the highest concentrations in emissions from burning red oak (Fig. 1a, b). The MS-MS spectrum of $C_{10}H_7NO_3$ (Fig. S4l) is like 2-nitro-1-phenol (Fig. S5g) but shows a ~1 min difference in retention time (Fig. S3i 10.9 min, 2-nitro-1-phenol 11.8 min). $C_{10}H_7NO_3$ is presumed to be an isomer of 2-nitro-1-phenol with a nitronaphthol structure. $C_{11}H_9NO_3$ has a degree of unsaturation and a fragmentation pattern (Fig. S4q) like $C_{10}H_7NO_3$ and is likely a structural isomer of methyl nitronaphthol. $C_6H_5NO_3$, $C_7H_7NO_3$, $C_6H_5NO_4$, and $C_7H_7NO_4$ are commonly detected in combustion emissions (Lin et al., 2016, 2017; Xie et al., 2019) and atmospheric particles (Claeys et al., 2012; Zhang et al., 2013). $C_6H_5NO_3$ and $C_6H_5NO_4$ are identified as 4-nitrophenol and 4-nitrocatechol using authentic standards (Figs. S4a, d and S5a, c). $C_7H_7NO_3$ has two isomers (Fig. S3b) and the compound eluting at 9.98 min has the same retention time and MS-MS spectrum (Fig. S4c) as 2-methyl-4-nitrophenol (Fig. S5b). In ambient PM and chamber SOA, $C_7H_7NO_4$ was identified using standard compounds as a series of methyl-nitrocatechol isomers (4-methyl-5-nitrocatechol, 3-methyl-5-nitrocatechol, and 3-methyl-6-nitrocatechol) (Iinuma et al., 2010). According to the HPLC-Q-ToFMS data for $C_7H_7NO_4$ identified in Iinuma et al. (2010) and our previous studies (Xie et al., 2017a, 2019), the two $C_7H_7NO_4$ isomers in Fig. S3d are likely 4-methyl-5-nitrocatechol and 3-methyl-6-nitrocatechol, respectively. Here we cannot rule out the presence of 3-methyl-5-nitrocatechol, which may co-elute with 4-methyl-5-nitrocatechol (Iinuma et al., 2010). In Fig. S4k, o, and p, the MS-MS spectra of $C_7H_7NO_5$, $C_8H_7NO_5$, and $C_8H_9NO_5$ all show a loss of CH_3 + NO (or NO_2) + CO. The loss of CH_3 is typically due to a methoxy group in NAC molecules, and NO (or NO_2) and CO loss is commonly observed for NACs with more than one phenoxy group (Xie et al., 2019). So methoxy nitrophenol is the proposed skeleton for $C_7H_7NO_5$, $C_8H_7NO_5$, and $C_8H_9NO_5$. Other functional groups were estimated using their chemical formulas and degree of unsaturation as a basis (Table S3).

The present study quantifies $C_8H_7NO_4$ and $C_9H_9NO_4$ using 2-methyl-5-benzoic acid ($C_8H_7NO_4$) and 2,5-dimethyl-4-nitrobenzoic acid ($C_9H_9NO_4$), respectively. The fragmentation patterns of $C_8H_7NO_4$ (Fig. S4g, h) and $C_9H_9NO_4$ compounds (Fig. S4m, n) are different from their corresponding surrogates (Fig. S5f, h) and loss of CO_2 is not observed, so $C_8H_7NO_4$ and $C_9H_9NO_4$ compound structures do not include a carboxyl group. The MS-MS spectra of $C_8H_7NO_4$ eluting at 8.14 min (Fig. S3e) and $C_9H_9NO_4$ eluting at 9.22 min (Fig. S3j) indicate the loss of OCN (Fig. S4g, m), suggesting benzoxazole/benzisoxazole structure or the presence of cyanate (—O—C≡N) or isocyanate (—O—C≡N) groups. Mass spectra of selected standard compounds (Fig. S5i-n) in our previous work (Xie et al. 2019) show the loss of an OCN group only happens during the fragmentation of phenyl cyanate. Thus, the $C_8H_7NO_4$ and $C_9H_9NO_4$ isomers containing OCN indicate a phenyl cyanate feature. However, the fragmentation mechanism related to the loss of a single nitrogen for the second $C_8H_7NO_4$ isomer (Figs. S3e and S4h) is unknown and requires further study. The MS-MS spectrum of the second $C_9H_9NO_4$ isomer had dominant ions at *m/z* 194 ($[M\text{-}H]^-$), 164 (loss of NO), and 149 (loss of NO + CH_3). Compared with the MS-MS spectra of 4-nitrophenol and 2-methyl-4-nitrophenol (Fig. S5a, b), the second $C_9H_9NO_4$ isomer is likely a methoxy nitrophenol with an extra ethyl group.

The EIC signal of $C_8H_9NO_4$ in Fig. S3f comprises at least 3-4 isomers, and the MS-MS spectra are always dominated by ions at m/z 182 ($[M–H]^-$), 152 (loss of NO), and 137 (loss

of NO + CH_3) with some changes in relative abundance. The fragmentation mechanism of $C_8H_9NO_4$ represented by the MS-MS spectrum in Fig. S4i is consistent with that of the second $C_9H_9NO_4$ isomer (Fig. S4n), so the $C_8H_9NO_4$ might also have a methoxy nitrophenol skeleton. The MS-MS spectrum of $C_8H_5NO_2$ is characterized by CO_2 loss (Fig. S4j), indicative of a carboxyl group. Considering the degree of unsaturation of the $C_8H_5NO_2$ molecule and the cyano group feature in BB tracers (e.g., hydrogen cyanide, benzonitrile) (Schneider et al., 1997; Li et al., 2000; Gilman et al., 2015), $C_8H_5NO_2$ was identified as 4-cyanobenzoic acid using authentic standard (Fig. S5o). The $C_{10}H_{11}NO_4$, $C_{10}H_{11}NO_5$, $C_{11}H_{13}NO_5$, and $C_{11}H_{13}NO_6$ detected here are also observed in other BB experiments (Xie et al., 2019). Their MS-MS spectra are characterized by the loss of at least one CH_3 and/or OCN (Fig. S4r-u), suggestive of methoxy or cyanate groups. Without authentic standards, fragmentation patterns (Fig. S4r-u) were used to determine the molecular structures of $C_{10}H_{11}NO_4$, $C_{10}H_{11}NO_5$, $C_{11}H_{13}NO_5$, and $C_{11}H_{13}NO_6$ (Table S3).

Nearly all NAC formulas identified in this work were observed previously (Lin et al., 2016, 2017; Xie et al., 2017a; Fleming et al., 2018; Xie et al., 2019). Few studies attempt to retrieve structural information for NACs using MS-MS spectra of authentic standards. Although multiple NACs may be generated from BB and photooxidation of aromatics in the presence of NO_X, NAC structures may differ across emission sources. Xie et al. (2019) found that fragmentation patterns of $C_7H_7NO_5$ and $C_8H_9NO_5$ from BB and photochemical reactions are distinct, and the methoxy and cyanate groups are featured only in BB NACs. Thus, knowing the NAC structure is useful to emissions source identification. In this work, the chemical and structural information obtained for NACs sampled during red oak and charcoal burning are similar, presumably because the charcoal fuel used is produced by the slow pyrolysis of wood. However, NACs in red oak and charcoal burning emissions can be differentiated compositionally. As shown in Figs. 1 and S2, the NAC emissions from red oak burning in cookstoves are characterized by $C_{10}H_7NO_3$ and $C_{11}H_9NO_3$. In addition to these two species, charcoal burning in cookstoves also generates high fractions of $C_8H_9NO_5$ (Fig. S2c, d). This difference among NACs may help with source apportionment using receptor models, which are commonly used and assume that the ambient pollutants measured in the field are linear combinations from a number of time-variant sources/factors. (Jaeckels et al., 2007; Shrivastava et al., 2007; Xie et al., 2013).

Figure 2 compares NAC composition from cookstove emissions (not including $C_8H_5NO_2$), open BB (Xie et al., 2019), and SOA chamber experiments (Xie et al., 2017a). Since previous source emissions studies ignored Q_b measurements and normalized individual NACs concentrations to OM, only Q_f measurements in this work are compared (Fig. 2a, b) with their $iNAC_{OC}$% values multiplied by 1.7 (proposed OM/OC ratio, Reff et al., 2009). The three open BB tests (Fig. 2c) were conducted with two fuel types under different ambient temperatures (10–29 °C) and RH% (49–83%) (Xie et al., 2019). But they consistently emit $C_6H_5NO_4$, $C_7H_7NO_4$, and $C_9H_9NO_4$, which is compositionally distinct from cookstove emissions (Fig. 2a, b). Moreover, the average mass contribution of total NACs to OM for open BB (0.12 ± 0.051%) was 4–14 times lower than that for cookstove emissions. This result is likely due to the high temperature flaming combustion produced in the cookstoves (Shen et al., 2012; Xie et al., 2018). In Fig. 2d and e, the NAC profiles yielded for photochemical reactions appear to have aromatic precursors. When using field

measurement data of NACs for receptor modeling, the resulting factors can be linked with specific emission sources by comparing with the NAC patterns shown in Fig. 2. Further studies are also warranted to unveil NAC patterns of other potential sources (e.g., motor vehicle emissions). Therefore, the source of NACs can be identified by combining their characteristic structures and composition. The filter-based NACs reported for the experiments shown in Fig. 2 were all measured using the identical method and HPLC-Q-ToFMS instrument, reducing any potential methodological bias. However, total gas-phase NAC concentrations need to be properly sampled and measured to account for the impact of gas/particle partitioning on their distribution.

3.4 Contributions of NACs to Abs_{365}

The average $Abs_{365,iNAC\%}$ values of Q_f and Q_b samples are presented by fuel type and WBT phase in the Fig. 3 stack plots, and experimental data for each fuel-cookstove are provided in Tables S11-S14. The average contributions of total NACs to Abs_{365} ($Abs_{365,tNAC}$%) of the sample extracts (Q_f 1.10 – 2.57%, Q_b 10.7 – 21.0%) are up to 10 times greater than their average $tNAC_{OC}$% (Q_f 0.31 – 1.01%, Q_b 1.08 – 3.31%, Table 1). Considering that some NACs are not light-absorbing (Table S4) and the OM/OC ratio is typically greater than unity, most NACs that contribute to Abs_{365} are strong BrC chromophores. Like the mass composition of NACs (Fig. 1), $C_{10}H_7NO_3$ (CS 0.24%, HS 0.43%) and $C_8H_9NO_5$ (CS 1.22%, HS 0.55%) were the major contributors to Abs_{365} for the Q_f samples collected during red oak and charcoal burning, respectively (Fig.3a). The average $Abs_{365,tNAC}$% of Q_b samples are 7.53 to 11.3 times higher than those of Q_f samples. Unlike the Q_f samples from red oak burning, $C_{10}H_{11}NO_5$ (CS 2.77%, HS 3.09%) has the highest average contribution to Abs_{365} for Q_b samples, followed by $C_{10}H_7NO_3$ (CS 1.96%, HS 1.32%) and $C_8H_9NO_5$ (CS 1.32%, HS 1.44%). While $C_8H_9NO_5$ dominated the contribution (CS 8.78%, HS 5.82%) to Abs_{365} for the Q_b samples from charcoal burning (Fig. 3b). All identified NACs explained 1.10 – 2.58% (Fig. S3) of Q_f extracts absorption. Even if the NACs on Q_b were totally derived from upstream filter evaporation, the adjusted average contributions of total NACs (Q_f + Q_b) to Abs_{365} of Q_f extracts were still lower than 5% (1.59 – 4.01%). Due to the lack of authentic standards, the quantification of NACs concentrations and their contributions to Abs_{365} of Q_f extracts might be subject to uncertainties. However, growing evidences showed that BrC absorption was majorly contributed by large molecules with MW > 500 – 1000 Da (Di Lorenzo and Young, 2016; Di Lorenzo et al., 2017). Large molecules of NACs may be generated from flaming combustions in cookstoves, and their structures and light absorption are worth future investigations. In previous studies on ambient and biomass burning particles, most identified NACs had a MW lower than 300 – 500 Da, and their total contributions to bulk BrC absorption were estimated to be less than 10% (Mohr et al., 2013; Zhang et al., 2013; Teich et al., 2017; Xie et al., 2019). Similar results were also obtained in the current work. Therefore, further studies are needed to identify large BrC molecules (including high MW NACs) in ambient and source particles.

4 Conclusion

This study investigated the composition, chemical formulas, and structures of NACs in $PM_{2.5}$ emitted from burning red oak and charcoal in a variety of cookstoves. Total NAC

mass and compositional differences between Q_f and Q_b samples suggest that the identified NACs might have substantial gas-phase concentrations. By comparing the MS-MS spectra of identified NACs to standard compound spectra, the structures of NACs featuring methoxy and cyanate groups in cookstove emissions are confirmed. The source identification of NACs would be less ambiguous if both the structures and composition of NACs are known, as different emission sources have distinct NAC characteristics. However, the compositional information of NACs based on Q_f measurements only are biased due to the lack of gas-phase data, and further studies are warranted to investigate the gas/particle distribution of NACs in the ambient and source emissions. Similar to previous work, the average contribution of total NACs to Abs_{365} of Q_f samples is less than 5% (1.10 – 2.57%), suggesting the need to shift our focus from low MW NACs (MW < 300 Da) to the chemical and optical properties of large molecules (e.g., MW > 500 Da) in particles.

Supplementary Material

Refer to Web version on PubMed Central for supplementary material.

Acknowledgements

This research was supported by the National Natural Science Foundation of China (NSFC, 41701551), the Startup Foundation for Introducing Talent of NUIST (No. 2243141801001), and in part by an appointment to the Postdoctoral Research Program at the Office of Research and Development by the Oak Ridge institute for Science and Education through Interagency Agreement No. 92433001 between the U.S. Department of Energy and the U.S. Environmental Protection Agency. We thank B. Patel for assistance on ECOC analysis of $PM_{2.5}$ filters.

Data availability

Data used in the writing of this manuscript is available at the U.S. Environmental Protection Agency's Environmental Dataset Gateway (https://edg.epa.gov).

References

Ahrens L, Harner T, Shoeib M, Lane DA, and Murphy JG: Improved characterization of gas–particle partitioning for per- and polyfluoroalkyl substances in the atmosphere using annular diffusion denuder samplers, Environmental Science & Technology, 46, 7199–7206, 10.1021/es300898s, 2012. [PubMed: 22606993]

Anenberg SC, Balakrishnan K, Jetter J, Masera O, Mehta S, Moss J, and Ramanathan V: Cleaner cooking solutions to achieve health, climate, and economic cobenefits, Environmental Science & Technology, 47, 3944–3952, 10.1021/es304942e, 2013. [PubMed: 23551030]

Aunan K, Berntsen TK, Myhre G, Rypdal K, Streets DG, Woo J-H, and Smith KR: Radiative forcing from household fuel burning in Asia, Atmospheric Environment, 43, 5674–5681, 10.1016/j.atmosenv.2009.07.053, 2009.

Bond TC, Streets DG, Yarber KF, Nelson SM, Woo J-H, and Klimont Z: A technology-based global inventory of black and organic carbon emissions from combustion, Journal of Geophysical Research: Atmospheres, 109, 10.1029/2003jd003697, 2004.

Bonjour S, Adair-Rohani H, Wolf J, Bruce Nigel G, Mehta S, Prüss-Ustün A, Lahiff M, Rehfuess Eva A, Mishra V, and Smith Kirk R: Solid fuel use for household cooking: Country and regional estimates for 1980–2010, Environmental Health Perspectives, 121, 784–790, 10.1289/ehp.1205987, 2013. [PubMed: 23674502]

Cao G, Zhang X, and Zheng F: Inventory of black carbon and organic carbon emissions from China, Atmospheric Environment, 40, 6516–6527, 10.1016/j.atmosenv.2006.05.070, 2006.

Chen Y, Sheng G, Bi X, Feng Y, Mai B, and Fu J: Emission factors for carbonaceous particles and polycyclic aromatic hydrocarbons from residential coal combustion in China, Environmental Science & Technology, 39, 1861–1867, 10.1021/es0493650, 2005. [PubMed: 15819248]

Chen Y, and Bond TC: Light absorption by organic carbon from wood combustion, Atmospheric Chemistry and Physics, 10, 1773–1787, 10.5194/acp-10-1773-2010, 2010.

Claeys M, Vermeylen R, Yasmeen F, Gómez-González Y, Chi X, Maenhaut W, Mészáros T, and Salma I: Chemical characterisation of humic-like substances from urban, rural and tropical biomass burning environments using liquid chromatography with UV/vis photodiode array detection and electrospray ionisation mass spectrometry, Environmental Chemistry, 9, 273–284, 10.1071/EN11163, 2012.

De Haan DO, Hawkins LN, Welsh HG, Pednekar R, Casar JR, Pennington EA, de Loera A, Jimenez NG, Symons MA, Zauscher M, Pajunoja A, Caponi L, Cazaunau M, Formenti P, Gratien A, Pangui E, and Doussin J-F: Brown carbon production in ammonium- or amine-containing aerosol particles by reactive uptake of methylglyoxal and photolytic cloud cycling, Environmental Science & Technology, 51, 7458–7466, 10.1021/acs.est.7b00159, 2017. [PubMed: 28562016]

Desyaterik Y, Sun Y, Shen X, Lee T, Wang X, Wang T, and Collett JL: Speciation of “brown” carbon in cloud water impacted by agricultural biomass burning in eastern China, Journal of Geophysical Research: Atmospheres, 118, 7389–7399, 10.1002/jgrd.50561, 2013.

Ding Y, Pang Y, and Eatough DJ: High-volume diffusion denuder sampler for the routine monitoring of fine particulate matter: I. Design and optimization of the PC-BOSS, Aerosol Science and Technology, 36, 369–382, 10.1080/027868202753571205, 2002.

Di Lorenzo RA, and Young CJ: Size separation method for absorption characterization in brown carbon: Application to an aged biomass burning sample, Geophysical Research Letters, 43, 458–465, 10.1002/2015gl066954, 2016.

Di Lorenzo RA, Washenfelder RA, Attwood AR, Guo H, Xu L, Ng NL, Weber RJ, Baumann K, Edgerton E, and Young CJ: Molecular-size-separated brown carbon absorption for biomass-burning aerosol at multiple field sites, Environmental Science & Technology, 51, 3128–3137, 10.1021/acs.est.6b06160, 2017. [PubMed: 28199090]

Donahue NM, Epstein SA, Pandis SN, and Robinson AL: A two-dimensional volatility basis set: 1. organic-aerosol mixing thermodynamics, Atmospheric Chemistry and Physics, 11, 3303–3318, 10.5194/acp-11-3303-2011, 2011.

Feng Y, Ramanathan V, and Kotamarthi VR: Brown carbon: a significant atmospheric absorber of solar radiation?, Atmospheric Chemistry and Physics, 13, 8607–8621, 10.5194/acp-13-8607-2013, 2013.

Fleming LT, Lin P, Laskin A, Laskin J, Weltman R, Edwards RD, Arora NK, Yadav A, Meinardi S, Blake DR, Pillarisetti A, Smith KR, and Nizkorodov SA: Molecular composition of particulate matter emissions from dung and brushwood burning household cookstoves in Haryana, India, Atmospheric Chemistry and Physics, 18, 2461–2480, 10.5194/acp-18-2461-2018, 2018.

Forrister H, Liu J, Scheuer E, Dibb J, Ziemba L, Thornhill KL, Anderson B, Diskin G, Perring AE, Schwarz JP, Campuzano-Jost P, Day DA, Palm BB, Jimenez JL, Nenes A, and Weber RJ: Evolution of brown carbon in wildfire plumes, Geophysical Research Letters, 42, 4623–4630, 10.1002/2015gl063897, 2015.

Gilman JB, Lerner BM, Kuster WC, Goldan PD, Warneke C, Veres PR, Roberts JM, de Gouw JA, Burling IR, and Yokelson RJ: Biomass burning emissions and potential air quality impacts of volatile organic compounds and other trace gases from fuels common in the US, Atmospheric Chemistry and Physics, 15, 13915–13938, 10.5194/acp-15-13915-2015, 2015.

Glarborg P, Jensen A, and Johnsson JE: Fuel nitrogen conversion in solid fuel fired systems, Progress in Energy and Combustion Science, 29, 89–113, 2003.

Global Alliance for Clean Cookstoves, 2014 Water Boiling Test (WBT) 4.2.3. Released 19 3 2014 http://cleancookstoves.org/technology-and-fuels/testing/protocols.html (accessed July 2017).

Harrison MA, Barra S, Borghesi D, Vione D, Arsene C, and Olariu RI: Nitrated phenols in the atmosphere: a review, Atmospheric Environment, 39, 231–248, 2005.

Hecobian A, Zhang X, Zheng M, Frank N, Edgerton ES, and Weber RJ: Water-soluble organic aerosol material and the light-absorption characteristics of aqueous extracts measured over the

Southeastern United States, Atmospheric Chemistry and Physics, 10, 5965–5977, 10.5194/acp-10-5965-2010, 2010.

Iinuma Y, Böge O, Gräfe R, and Herrmann H: Methyl-nitrocatechols: Atmospheric tracer compounds for biomass burning secondary organic aerosols, Environmental Science & Technology, 44, 8453–8459, 10.1021/es102938a, 2010. [PubMed: 20964362]

International Agency for Research on Cancer (IARC): Some non-heterocyclic polycyclic aromatic hydrocarbons and some related exposures (Vol. 92). IARC Press, International Agency for Research on Cancer, 2010.

Jaeckels JM, Bae MS, and Schauer JJ: Positive matrix factorization (PMF) analysis of molecular marker measurements to quantify the sources of organic aerosols, Environmental Science & Technology, 41, 5763–5769, 10.1021/es062536b, 2007. [PubMed: 17874784]

Jetter JJ, and Kariher P: Solid-fuel household cook stoves: Characterization of performance and emissions, Biomass and Bioenergy, 33, 294–305, 10.1016/j.biombioe.2008.05.014, 2009.

Jetter J, Zhao Y, Smith KR, Khan B, Yelverton T, DeCarlo P, and Hays MD: Pollutant emissions and energy efficiency under controlled conditions for household biomass cookstoves and implications for metrics useful in setting international test standards, Environmental Science & Technology, 46, 10827–10834, 10.1021/es301693f, 2012. [PubMed: 22924525]

Kaal J, Martínez Cortizas A, and Nierop KGJ: Characterisation of aged charcoal using a coil probe pyrolysis-GC/MS method optimised for black carbon, Journal of Analytical and Applied Pyrolysis, 85, 408–416, 10.1016/j.jaap.2008.11.007, 2009.

Kim K-H, Jahan SA, Kabir E, and Brown RJC: A review of airborne polycyclic aromatic hydrocarbons (PAHs) and their human health effects, Environment International, 60, 71–80, 10.1016/j.envint.2013.07.019, 2013. [PubMed: 24013021]

Kim Oanh NT, Bstz Reutergårdh L, and Dung NT: Emission of polycyclic aromatic hydrocarbons and particulate matter from domestic combustion of selected fuels, Environmental Science & Technology, 33, 2703–2709, 10.1021/es980853f, 1999.

Kirchstetter TW, Corrigan CE, and Novakov T: Laboratory and field investigation of the adsorption of gaseous organic compounds onto quartz filters, Atmospheric Environment, 35,1663–1671, 10.1016/S1352-2310(00)00448-9, 2001.

Klimont Z, Cofala J, Xing J, Wei W, Zhang C, Wang S, Kejun J, Bhandari P, Mathur R, Purohit P, Rafaj P, Chambers A, Amann M, and Hao J: Projections of SO2, NO_X and carbonaceous aerosols emissions in Asia, Tellus B, 61, 602–617, 10.1111/j.l600-0889.2009.00428.x, 2009.

Kwamena N-O, and Abbatt J: Heterogeneous nitration reactions of polycyclic aromatic hydrocarbons and n-hexane soot by exposure to NO3/NO2/N2O5, Atmospheric Environment, 42, 8309–8314, 2008.

Lacey F, and Henze D: Global climate impacts of country-level primary carbonaceous aerosol from solid-fuel cookstove emissions, Environmental Research Letters, 10, 114003, 10.1088/1748-9326/10/11/114003, 2015.

Lei Y, Zhang Q, He KB, and Streets DG: Primary anthropogenic aerosol emission trends for China, 1990–2005, Atmospheric Chemistry and Physics, 11, 931–954, 10.5194/acp-11-931-2011, 2011.

Li Q, Jacob DJ, Bey I, Yantosca RM, Zhao Y, Kondo Y, and Notholt J: Atmospheric hydrogen cyanide (HCN): Biomass burning source, ocean sink?, Geophysical Research Letters, 27, 357–360, 10.1029/1999gl010935, 2000.

Lin P, Aiona PK, Li Y, Shiraiwa M, Laskin J, Nizkorodov SA, and Laskin A: Molecular characterization of brown carbon in biomass burning aerosol particles, Environmental Science & Technology, 50, 11815–11824, 10.1021/acs.est.6b03024, 2016. [PubMed: 27704802]

Lin P, Bluvshtein N, Rudich Y, Nizkorodov SA, Laskin J, and Laskin A: Molecular chemistry of atmospheric brown carbon inferred from a nationwide biomass burning event, Environmental Science & Technology, 51, 11561–11570, 10.1021/acs.est.7b02276, 2017. [PubMed: 28759227]

Lin P, Liu JM, Shilling JE, Kathmann SM, Laskin J, and Laskin A: Molecular characterization of brown carbon (BrC) chromophores in secondary organic aerosol generated from photo-oxidation of toluene, Physical Chemistry Chemical Physics, 17, 23312–23325, 10.1039/c5cp02563j, 2015. [PubMed: 26173064]

Liu J, Bergin M, Guo H, King L, Kotra N, Edgerton E, and Weber RJ: Size-resolved measurements of brown carbon in water and methanol extracts and estimates of their contribution to ambient fine-particle light absorption, Atmospheric Chemistry and Physics, 13, 12389–12404, 10.5194/acp-13-12389-2013, 2013.

Lu C, Wang X, Li R, Gu R, Zhang Y, Li W, Gao R, Chen B, Xue L, and Wang W: Emissions of fine particulate nitrated phenols from residential coal combustion in China, Atmospheric Environment, 203, 10–17, 10.1016/j.atmosenv.2019.01.047, 2019.

Lu JW, Flores JM, Lavi A, Abo-Riziq A, and Rudich Y: Changes in the optical properties of benzo[a]pyrene-coated aerosols upon heterogeneous reactions with NO2 and NO3, Physical Chemistry Chemical Physics, 13, 6484–6492, 10.1039/C0CP02114H, 2011. [PubMed: 21373662]

Lu Z, Streets DG, Winijkul E, Yan F, Chen Y, Bond TC, Feng Y, Dubey MK, Liu S, Pinto JP, and Carmichael GR: Light absorption properties and radiative effects of primary organic aerosol emissions, Environmental Science & Technology, 49, 4868–4877, 10.1021/acs.est.5b00211, 2015. [PubMed: 25811601]

McMeeking G, Fortner E, Onasch T, Taylor J, Flynn M, Coe H, and Kreidenweis S: Impacts of nonrefractory material on light absorption by aerosols emitted from biomass burning, Journal of Geophysical Research: Atmospheres, 119, 12,272–212,286, 2014.

Mohr C, Lopez-Hilfiker FD, Zotter P, Prévôt ASH, Xu L, Ng NL, Herndon SC, Williams LR, Franklin JP, Zahniser MS, Worsnop DR, Knighton WB, Aiken AC, Gorkowski KJ, Dubey MK, Allan JD, and Thornton JA: Contribution of nitrated phenols to wood burning brown carbon light absorption in Detling, United Kingdom during winter time, Environmental Science & Technology, 47, 6316–6324, 10.1021/es400683v, 2013. [PubMed: 23710733]

Nakayama T, Matsumi Y, Sato K, Imamura T, Yamazaki A, and Uchiyama A: Laboratory studies on optical properties of secondary organic aerosols generated during the photooxidation of toluene and the ozonolysis of α-pinene, Journal of Geophysical Research: Atmospheres, 115, n/a-n/a, 10.1029/2010jd014387, 2010.

Park RJ, Kim MJ, Jeong JI, Youn D, and Kim S: A contribution of brown carbon aerosol to the aerosol light absorption and its radiative forcing in East Asia, Atmospheric Environment, 44, 1414–1421, 10.1016/j.atmosenv.2010.01.042, 2010.

Peters AJ, Lane DA, Gundel LA, Northcott GL, and Jones KC: A comparison of high volume and diffusion denuder samplers for measuring semivolatile organic compounds in the atmosphere, Environmental Science & Technology, 34, 5001–5006, 10.1021/es000056t, 2000.

Pokhrel RP, Wagner NL, Langridge JM, Lack DA, Jayarathne T, Stone EA, Stockwell CE, Yokelson RJ, and Murphy SM: Parameterization of single-scattering albedo (SSA) and absorption Ångström exponent (AAE) with EC / OC for aerosol emissions from biomass burning, Atmospheric Chemistry and Physics, 16, 9549–9561, 10.5194/acp-16-9549-2016, 2016.

Ravindra K, Sokhi R, and Van Grieken R: Atmospheric polycyclic aromatic hydrocarbons: Source attribution, emission factors and regulation, Atmospheric Environment, 42, 2895–2921, 10.1016/j.atmosenv.2007.12.010, 2008.

Reff A, Bhave PV, Simon H, Pace TG, Pouliot GA, Mobley JD, and Houyoux M: Emissions inventory of PM2.5 trace elements across the United States, Environmental Science & Technology, 43, 5790–5796, 10.1021/es802930x, 2009. [PubMed: 19731678]

Riddle SG, Jakober CA, Robert MA, Cahill TM, Charles MJ, and Kleeman MJ: Large PAHs detected in fine particulate matter emitted from light-duty gasoline vehicles, Atmospheric Environment, 41, 8658–8668, 10.1016/j.atmosenv.2007.07.023, 2007.

Saleh R, Robinson ES, Tkacik DS, Ahern AT, Liu S, Aiken AC, Sullivan RC, Presto AA, Dubey MK, Yokelson RJ, Donahue NM, and Robinson AL: Brownness of organics in aerosols from biomass burning linked to their black carbon content, Nature Geoscience, 7, 647–650, 10.1038/ngeo2220, 2014.

Samburova V, Connolly J, Gyawali M, Yatavelli RLN, Watts AC, Chakrabarty RK, Zielinska B, Moosmüller H, and Khlystov A: Polycyclic aromatic hydrocarbons in biomass-burning emissions and their contribution to light absorption and aerosol toxicity, Science of The Total Environment, 568, 391–401, 10.1016/j.scitotenv.2016.06.026, 2016.

Schneider J, Bürger V, and Arnold F: Methyl cyanide and hydrogen cyanide measurements in the lower stratosphere: Implications for methyl cyanide sources and sinks, Journal of Geophysical Research: Atmospheres, 102, 25501–25506, 10.1029/97jd02364, 1997.

Shen G, Tao S, Wei S, Zhang Y, Wang R, Wang B, Li W, Shen H, Huang Y, Chen Y, Chen H, Yang Y, Wang W, Wei W, Wang X, Liu W, Wang X, and Simonich SLM: Reductions in Emissions of Carbonaceous particulate matter and polycyclic aromatic hydrocarbons from combustion of biomass pellets in comparison with raw fuel burning, Environmental Science & Technology, 46, 6409–6416, 10.1021/es300369d, 2012. [PubMed: 22568759]

Shrivastava MK, Subramanian R, Rogge WF, and Robinson AL: Sources of organic aerosol: Positive matrix factorization of molecular marker data and comparison of results from different source apportionment models, Atmospheric Environment, 41, 9353–9369, 10.1016/j.atmosenv.2007.09.016, 2007.

Simoneit BR, Rogge W, Mazurek M, Standley L, Hildemann L, and Cass G: Lignin pyrolysis products, lignans, and resin acids as specific tracers of plant classes in emissions from biomass combustion, Environmental science & technology, 27, 2533–2541, 1993.

Simoneit BR: Biomass burning—a review of organic tracers for smoke from incomplete combustion, Applied Geochemistry, 17, 129–162, 2002.

Smith KR, Bruce N, Balakrishnan K, Adair-Rohani H, Balmes J, Chafe Z, Dherani M, Hosgood HD, Mehta S, Pope D, and Rehfuess E: Millions dead: How do we know and what does it mean? Methods used in the comparative risk assessment of household air pollution, Annual Review of Public Health, 35, 185–206, 10.1146/annurev-publhealth-032013-182356, 2014.

Subramanian R, Khlystov AY, Cabada JC, and Robinson AL: Positive and negative artifacts in particulate organic carbon measurements with denuded and undenuded sampler configurations special issue of Aerosol Science and Technology on findings from the fine particulate matter supersites program, Aerosol Science and Technology, 38, 27–48, 10.1080/02786820390229354, 2004.

Sun J, Zhi G, Hitzenberger R, Chen Y, Tian C, Zhang Y, Feng Y, Cheng M, Cai J, Chen F, Qiu Y, Jiang Z, Li J, Zhang G, and Mo Y: Emission factors and light absorption properties of brown carbon from household coal combustion in China, Atmospheric Chemistry and Physics, 17,4769–4780, 10.5194/acp-17-4769-2017, 2017.

Teich M, van Pinxteren D, Wang M, Kecorius S, Wang Z, Müller T, Močnik G, and Herrmann H: Contributions of nitrated aromatic compounds to the light absorption of water-soluble and particulate brown carbon in different atmospheric environments in Germany and China, Atmospheric Chemistry and Physics, 17, 1653–1672, 10.5194/acp-17-1653-2017, 2017.

Tuccella P, Curci G, Pitari G, Lee S, and Jo DS: Direct radiative effect of absorbing aerosols: sensitivity to mixing state, brown carbon and soil dust refractive index and shape, Journal of Geophysical Research: Atmospheres, 125, e2019JD030967, 10.1029/2019JD030967, 2020.

Turpin BJ, and Lim H-J: Species contributions to PM2.5 mass concentrations: Revisiting common assumptions for estimating organic mass, erosol Science and Technology, 35, 602–610, 10.1080/02786820119445, 2001.

Wang X, Heald CL, Ridley DA, Schwarz JP, Spackman JR, Perring AE, Coe H, Liu D, and Clarke AD: Exploiting simultaneous observational constraints on mass and absorption to estimate the global direct radiative forcing of black carbon and brown carbon, Atmospheric Chemistry and Physics, 14, 10989–11010, 10.5194/acp-14-10989-2014, 2014.

Wathore R, Mortimer K, and Grieshop AP: In-use emissions and estimated impacts of traditional, natural- and forced-draft cookstoves in rural Malawi, Environmental Science & Technology, 51, 1929–1938, 10.1021/acs.est.6b05557, 2017. [PubMed: 28060518]

Watson JG, Chow JC, Chen LWA, and Frank NH: Methods to assess carbonaceous aerosol sampling artifacts for IMPROVE and other long-term networks, Journal of the Air & Waste Management Association, 59, 898–911, 10.3155/1047-3289.59.8.898, 2009. [PubMed: 19728484]

Xie M, Hannigan MP, Dutton SJ, Milford JB, Hemann JG, Miller SL, Schauer JJ, Peel JL, and Vedal S: Positive matrix factorization of PM2.5: Comparison and implications of using different speciation data sets, Environmental Science & Technology, 46, 11962–11970, 10.1021/es302358g, 2012. [PubMed: 22985292]

Xie M, Hannigan MP, and Barsanti KC: Gas/particle partitioning of n-alkanes, PAHs and oxygenated PAHs in urban Denver, Atmospheric Environment, 95, 355–362, 10.1016/j.atmosenv.2014.06.056, 2014.

Xie M, Chen X, Hays MD, Lewandowski M, Offenberg J, Kleindienst TE, and Holder AL: Light absorption of secondary organic aerosol: Composition and contribution of nitroaromatic compounds, Environmental Science & Technology, 51, 11607–11616, 10.1021/acs.est.7b03263, 2017a. [PubMed: 28930472]

Xie M, Hays MD, and Holder AL: Light-absorbing organic carbon from prescribed and laboratory biomass burning and gasoline vehicle emissions, Scientific Reports, 7, 7318, 10.1038/s41598-017-06981-8, 2017b. [PubMed: 28779152]

Xie M, Shen G, Holder AL, Hays MD, and Jetter JJ: Light absorption of organic carbon emitted from burning wood, charcoal, and kerosene in household cookstoves, Environmental Pollution, 240, 60–67, 10.1016/j.envpol.2018.04.085, 2018. [PubMed: 29729570]

Xie M, Chen X, Hays MD, and Holder AL: Composition and light absorption of N-containing aromatic compounds in organic aerosols from laboratory biomass burning, Atmospheric Chemistry and Physics, 19, 2899–2915, 10.5194/acp-19-2899-2019, 2019. [PubMed: 31501655]

Xie M, Piedrahita R, Dutton SJ, Milford JB, Hemann JG, Peel JL, Miller SL, Kim S-Y, Vedal S, Sheppard L, and Hannigan MP: Positive matrix factorization of a 32-month series of daily PM2.5 speciation data with incorporation of temperature stratification, Atmospheric Environment, 65, 11–20, 10.1016/j.atmosenv.2012.09.034, 2013. [PubMed: 25214809]

Yang M, Howell SG, Zhuang J, and Huebert BJ: Attribution of aerosol light absorption to black carbon, brown carbon, and dust in China – interpretations of atmospheric measurements during EAST-AIRE, Atmospheric Chemistry and Physics, 9, 2035–2050, 10.5194/acp-9-2035-2009, 2009.

Zhang X, Lin Y-H, Surratt JD, and Weber RJ: Sources, composition and absorption Ångström exponent of light-absorbing organic components in aerosol extracts from the Los Angeles basin, Environmental Science & Technology, 47, 3685–3693, 10.1021/es305047b, 2013. [PubMed: 23506531]

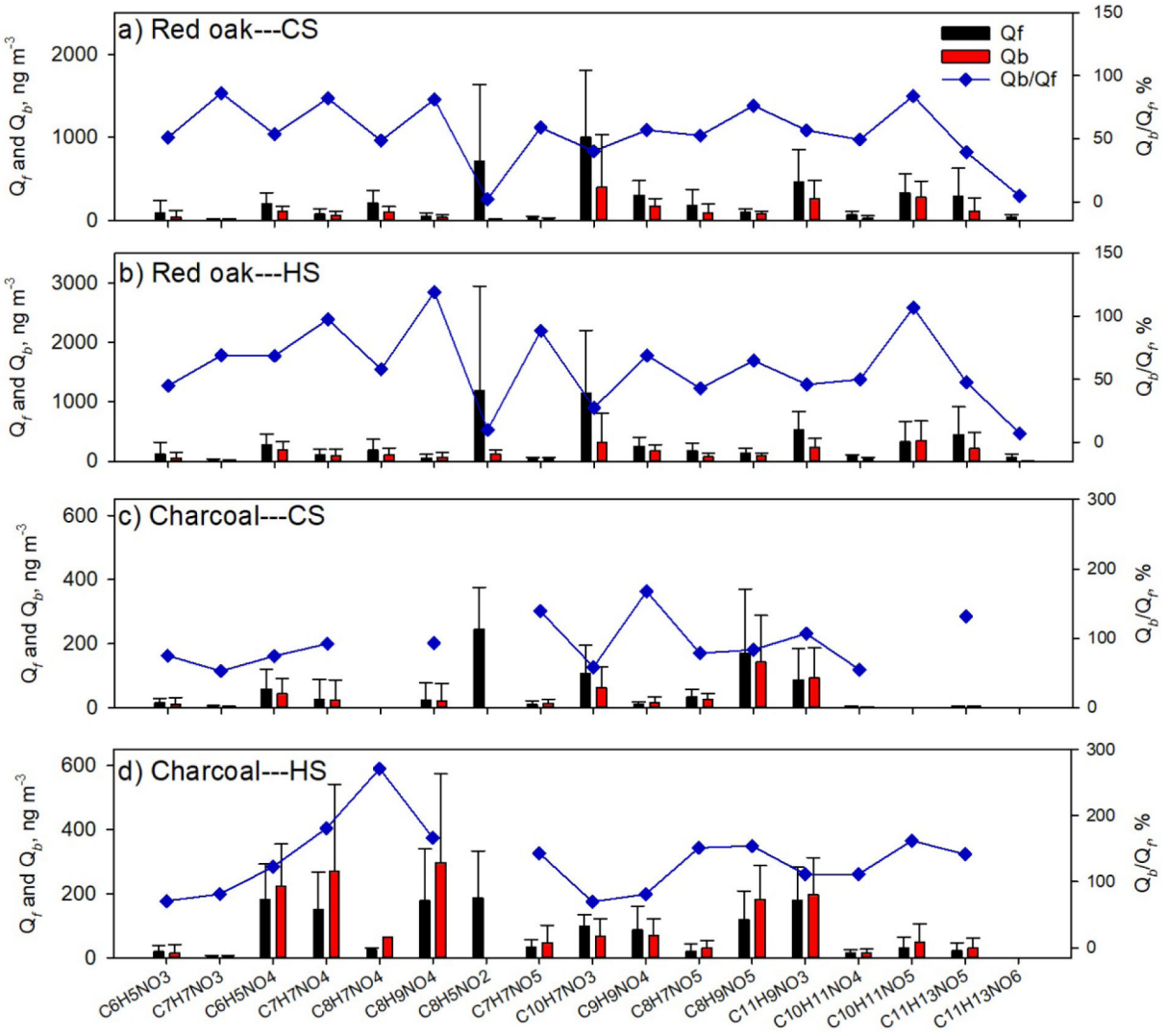

Figure 1.

Average concentrations of individual NACs in Q_f and Q_b samples for (a) red oak burning under the CS phase, (b) red oak burning under the HS phase, (c) charcoal burning under the CS phase, and (d) charcoal burning under the HS phase. The blue scatters in each plot are mass ratios of individual NACs in Q_b to Q_f samples × 100%.

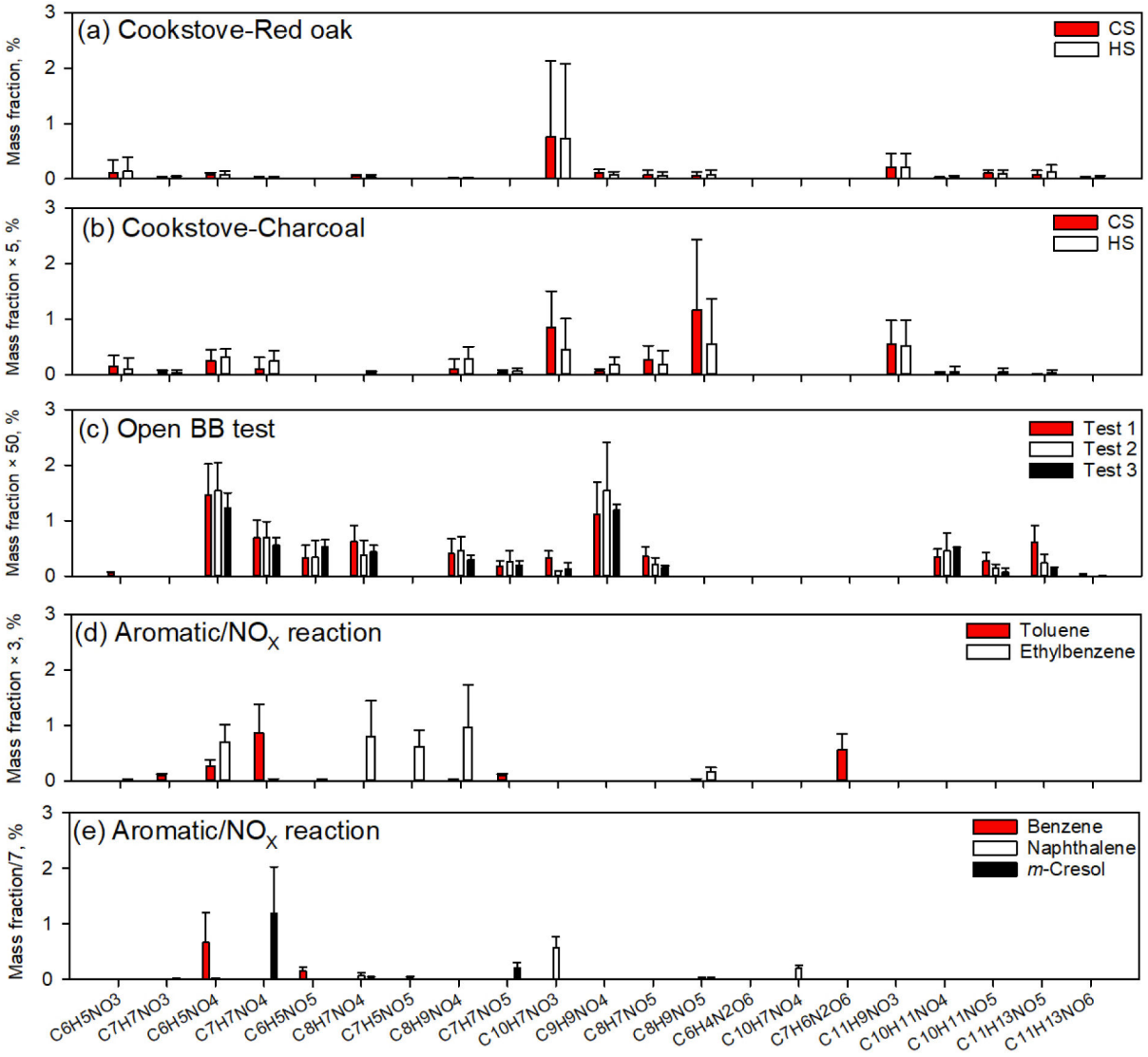

Figure 2.

Average mass ratios (%) of individual NACs to organic matter from (a) red oak burning in cookstoves, (b) charcoal burning in cookstoves, (c) open BB experiments (Xie et al., 2019), photochemical reactions of (d) toluene and ehthylbenzene, and (e) benzene, naphthalene, and m-cresol with NO_X (Xie et al., 2017a).

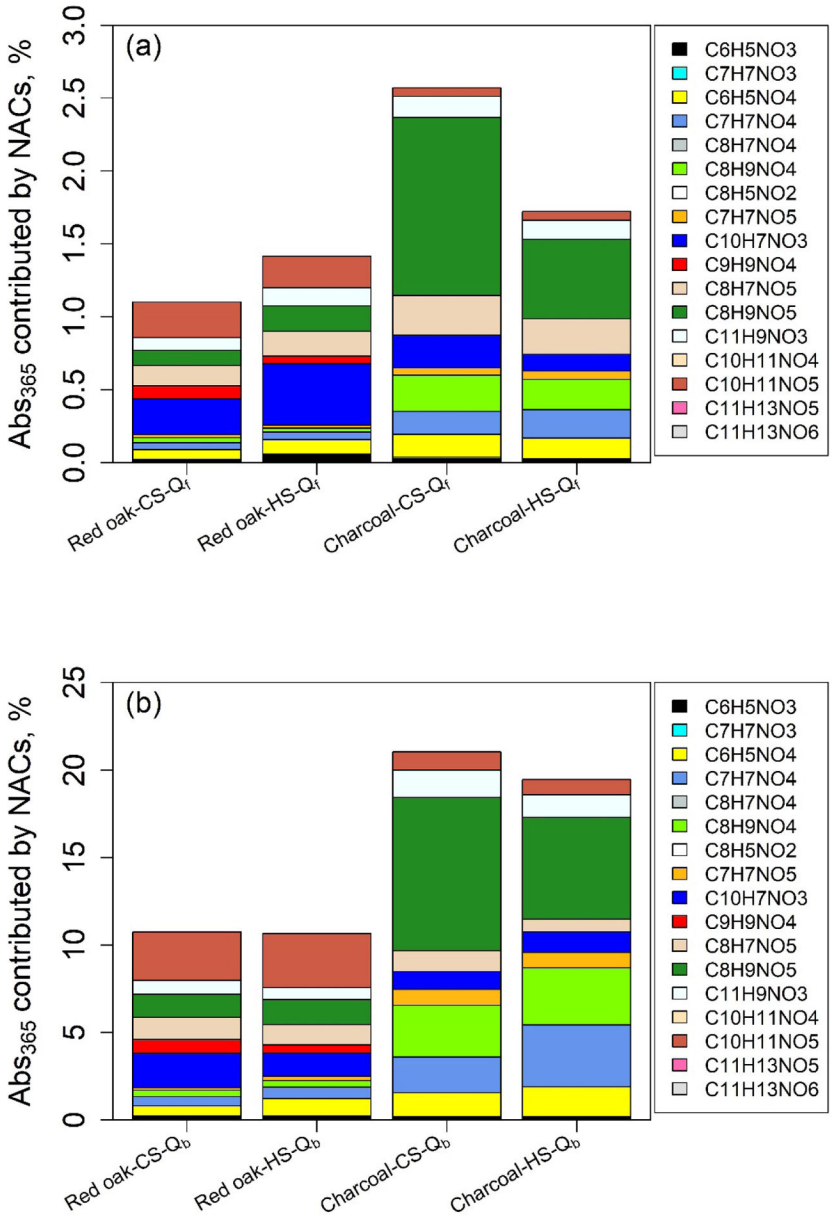

Figure 3.

Average contributions (%) of individual NACs to bulk extracts Abs_{365} of (a) Q_f, and (b) Q_b samples from burning red oak and charcoal in cookstoves under CS and HS phases.

Table 1.

Average concentrations of total NACs and $tNAC_{OC}$% in Q_f and Q_b samples by fuel type and WBT phase.

Fuel & Test phase	Red Oak		Charcoal	
	CS	HS[a]	CS	HS
Front filter (Q_f)				
Sample number	18	17[b]	15	15
total NAC (μg m^{-3})	3.43 ± 1.37	3.91 ± 2.06	0.51 ± 0.43	1.00 ± 0.48
$tNAC_{OC}$%	1.01 ± 1.06	0.98 ± 1.09	0.40 ± 0.25	0.31 ± 0.21
OC (μg m^{-3})[c]	624 ± 410	908 ± 885	115 ± 72.0	447 ± 271
EC/OC[c]	1.74 ± 1.42	1.96 ± 1.74	6.12 ± 2.76	0.029 ± 0.012
Backup filter (Q_b)				
Sample number	18	17[b]	14[b]	15
total NAC (μg m^{-3})	1.67 ± 0.76	1.79 ± 0.77	0.37 ± 0.31	1.30 ± 0.70
$tNAC_{OC}$%	3.31 ± 3.46	2.77 ± 2.66	1.10 ± 0.89	1.08 ± 0.51
OC (μg m^{-3})[c]	78.4 ± 43.2	100 ± 58.4	41.9 ± 23.3	138 ± 70.8
Q_b/Q_f ratio (%)				
total NACs	50.8 ± 13.4	53.4 ± 26.2	84.1 ± 38.0	140 ± 52.9
OC[c]	14.8 ± 3.87	15.3 ± 6.37	35.4 ± 12.2	38.8 ± 18.9

[a] Including three SIM phase samples from the 3-stone fire

[b] one filter sample was missed for analysis

[c] data were obtained from Xie et al. (2018).